Astron. Astrophys. 334, 363–375 (1998)

ASTRONOMY AND ASTROPHYSICS

Molecular dynamics simulation of the H_2 recombination on a graphite surface

P. Parneix and Ph. Bréchignac

Laboratoire de Photophysique Moléculaire*, C.N.R.S. Bât 210, Université de Paris-Sud, F-91405 Orsay Cedex, France
(philippe.brechignac@ppm.u-psud.fr)

Received 4 August 1997 / Accepted 22 January 1998

Abstract. This article reports a model study aimed at the detailed description of the mechanism of formation of molecular hydrogen onto dust grain surfaces in the interstellar medium. Using classical trajectories (CT) and quasi-classical trajectories (QCT) calculations, the H_2 recombination from the Eley-Rideal process has been studied. This reactive process, involving the collision between one gas phase atomic hydrogen and one other H atom previously chemisorbed on a graphite surface, could be an efficient mechanism to explain the formation of H_2 in the interstellar medium. Two empirical potential models have been used to extract the main physical and chemical properties of this system. The efficiency of the recombination process has been analysed as a function of the collision energy and also as a function of the H coverage on the graphite surface. From an energetic point of view, the newly formed H_2 molecules have been found to be desorbed with a large translation kinetic energy and also in highly excited vibrational states.

Key words: dust, extinction – ISM: molecules – molecular processes

1. Introduction

1.1. General

The detailed mechanism for the formation of the H_2 molecule in the interstellar medium (ISM) really appears to stand up to now as an open question for astrophysicists. Indeed the strong abundance of H_2 in the ISM cannot be explained by the classical three-body collisions due to the very low density of the interstellar gas (about 10^2 - 10^4 atoms/cm^3 for a typical temperature of about $10^1 - 10^2$K) nor by the appropriate mechanisms usually at work in space, like radiative association. Consequently astrophysicists have been interested for a long time in the dynamical processes which could induce a high efficiency of the H_2 formation in such a rarefied medium.

One another fundamental point for the understanding of the chemical evolution of the ISM is the redistribution of available energy in the nascent H_2 molecules. Indeed part of this energy could go into H_2 vibration or/and rotation. On the other hand UV radiation from the stars induces electronic transitions to the $B^1\Sigma_u^+$ (Lyman band) and $C^1\Pi_u$ (Werner band) electronic states. These two electronic states lead to the destruction of the H_2 molecule by spontaneous radiative dissociation (coupling to the nuclear continuum) with an efficiency of about 10 % (Stephens & Dalgarno 1972; Schmoranzer et al. 1990). But they also radiatively de-excite to bound rovibrational states of the ground electronic state $X^1\Sigma_g^+$. This process, known as the UV pumping, prepares population in highly excited rovibrational levels in the ground $X^1\Sigma_g^+$ which then cascade down by infrared (IR) emission. The spectrum and intensity of the IR radiation, now currently observed from both ground-based (Burton et al. 1992; Brand 1993; Field et al. 1994; Lemaire et al. 1996; Rouan et al. 1997; Sugai et al. 1997) and space-based ISO telescopes, will naturally depend on the UV radiation flux but also on the initial rovibrational population of the nascent H_2 molecule, as recently demonstrated by Le Bourlot et al. (1995). Burton et al. (1992) have proposed that the formation mechanism could be at the origin of the excess IR emission observed in the NGC2023 reflection nebula. Futhermore information about the energy released into translation of H_2 is important since it can contribute to the heating of the gas in diffuse clouds (Jura 1976).

As the presence of small particles (*interstellar dust* or *grains*) in the ISM is now well established (mainly through the spectral analysis of the extinction curve and by their typical infrared signature), reactive processes at the gas-solid interface have been proposed as an altervative solution to explain the H_2 recombination (Hollenbach & Salpeter 1970,1971; Jura 1975, Watson 1976; Goodman 1978). Astrophysical implications of these gas-surface interactions have been widely discussed through different models (Black & Dalgarno 1976; Hunter & Watson 1978; Duley & Williams 1986, 1993; Dalgarno 1993). Unfortunately the chemical nature, the size and the structure of these pieces of solid and the density of such material are not well characterized yet. Most recent results on the exctinction of dense regions in the infrared part of the spectrum, obtained thanks to ISO satellite (Abergel et al., private communication), show that the grain model proposed by Draine & Lee (1984) accounts well for the main features: absorption near 10 μm by the silicates component of the grain distribution, and gradual rise towards shorter wavelengths due to the graphite component. Indeed the graphite character of a significant pro-

* Laboratoire associé à l'université Paris-Sud

portion of the grains is also attested by the so-called "UV-bump" at 217 nm, as first suggested by Mathis et al. (1977) and later quantified in various ways by many authors (see in particular Fitzpatrick et al. (1990)). This presence of graphite has been our motivation for the present study: a microscopic description of the H_2 formation near a "perfect" graphite surface. We have to keep in mind that the chemical reaction studied in this work (graphite+H+H—> graphite +H_2) has to be considered as a model system for the ISM to extract general trends. In the ISM, the reality is obviously more complex due to different factors which can strongly affect the cross-sections associated to the reactive processes. For example the presence of condensable molecules (H_2O, CO, CO_2...) on the surface of the dust particles in the molecular clouds (characterized by low temperature and low radiation flux) can induce strong changes in the electronic structure and consequently in the reactivity on these surfaces. Another important point to mention is that the structure (planar, spherical,...) of the grains and the eventual presence of defects on the surface could also play a crucial role in such reactive processes.

As the microscopic detailed mechanism of surface recombination is concerned, two schematic descriptions are generally proposed to explain the formation of a chemically bound system, here H_2 near a surface. The first one, called the Langmuir-Hinschelwood (LH) mechanism assumes that the atomic reactants are already adsorbed on the surface. The adsorbates then migrate from site to site until they react upon encounter. The final product is then desorbed to the gaseous phase. In this process, reactivity occurs between two atoms already adsorbed and thermalized by the surface. Consequently, the reactivity will be strongly dependent on the surface temperature and coverage.

The second one, called the Eley-Rideal (ER) mechanism, corresponds to the process studied in this work. It is a direct interaction in which a reactive collision occurs between a gas phase atom and an adsorbed atom. If this adsorbed H atom is rather localized on the surface, we can expect that the reactivity will be less dependent on the surface temperature than in the LH mechanism. It is important to note that the energetics of the reaction will be different in the two processes due to the difference in the initial state of one of the reactants. Indeed the formation energy (ΔE) is equal to $E^{(H_2)}$ - $E^{(H)}$ in the ER process while this energy is smaller and equal to $E^{(H_2)}$ - 2 $E^{(H)}$ in the LH process. $E^{(H)}$ and $E^{(H_2)}$ are respectively the binding energies of H and H_2 on the graphite surface.

Both processes pre-suppose the existence of a non negligible atomic coverage on the grain surface to take place. It is then of interest to address the question of the nature of the adsorption sites which are occupied in relation to astrophysical conditions. The binding energy for an H atom on graphite can be estimated to about 1.2 eV in a chemisorption site (Fromherz et al. 1993) and to about 50 meV in a physisorption site (Mattera et al. 1980). If we don't consider the chemical reaction induced desorption, the atomic coverage is the result of the competition between the sticking of H-atoms coming from the gas phase and the thermal desorption. The efficiency of this process has a very strong temperature dependence. For typical conditions of the gas phase in interstellar clouds (density $n_H \approx 1000$ cm^{-3}, gas temperature $Tg \approx 100$ K) it can be estimated that desorption will overcome sticking as soon as the grain temperature T_d is larger than 12 K for physisorption and 300 K for chemisorption. Thus for moderately dense interstellar clouds with T_d = 15-40 K we expect a significant chemisorption coverage and negligible physisorption. The typical time scale for the construction of the coverage is rather short ($\approx$ 1 year).

1.2. The Eley-Rideal process

The LH mechanism is not the goal of this work. It will only be considered in the context of the discussion of astrophysical conditions.

In the ER process, studied here, three different exit channels are possible. The first one corresponds to the formation of the H_2 molecule and its desorption to the gas phase. In this case, we will speak about reactive trajectories. This process can be summarized as:

$$(Surface...H) + H(\epsilon_t) \longrightarrow Surface \ + \ H_2(\epsilon'_t, v, j)$$

It is important to note that this process can be direct or not. Indeed, during its trajectrory, the incoming H atom can be trapped on the surface, then diffuses more or less easily (depending on its translational kinetic energy) and eventually reacts after a long time. This indirect process is taken into account in the present simulation because the H adsorbed atom is initially located in a given (x,y) cell with periodic boundary conditions. It means that the simulated process corresponds in fact to the reactive collision between a H atom and a hydrogenated surface defined by a density of adsorbates per unit area, i.e. a coverage.

The second one corresponds to the collision of the H atom without involving chemical reaction. In this case, the H atom comes back to the gas phase after elastic and/or inelastic scattering. Such trajectories, which can be summarized as:

$$(Surface...H) + H(\epsilon_t) \longrightarrow (Surface...H) \ + \ H(\epsilon'_t)$$

will be referred to as non-reactive.

The third one corresponds to the sticking of the incoming H atom:

$$(Surface...H) + H(\epsilon_t) \longrightarrow (Surface...H...H)^*$$

This last process involves a coupling between the hydrogen atoms and the surface, which implies that energy transfer towards the bulk solid is possible. It will not be considered in the present work, for which the surface is assumed to be rigid.

From the experimental point of view, it is not easy to distinguish between the different mechanisms for various reasons. The first difficulty is for discreminating the nascent molecules from undissociated hydrogen molecules in the incoming beam or background gas. The second one is related to the actual state of the surface, in particular with respect to H and/or H_2 adsorption. The smaller or larger coverage may affect the relative importance of LH versus ER mechanisms. These mechanisms have been investigated mainly on metallic surfaces (Rettner &

Auerbach 1994; Rettner 1994; Schermann et al. 1994; Rettner & Auerbach 1996). Only very few experiments have been done on H_2 formation from a gas-surface interaction in which the surface could be representative of an interstellar dust grain. In the recent experiments by Pironnello et al. (1997) the discrimination of products from reactants was achieved by detecting HD scattered from an olivine slab at very low temperature irradiated by two independent H and D gas lines. Evidence for the LH mechanism was found. A major interest of the experiments performed by Gough et al. (1996) on carbonaceous materials is to give access to the internal state distribution of the H_2 product by means of an original technique. But the surface structure and exact content of the reactant gas is less securely characterized.

On the theoretical side, time-dependent fully-quantum calculations have been performed to describe the ER mechanism leading to the H_2 molecule formation on a metallic copper surface Cu(111) in a collinear collision (Jackson & Persson 1992a,1992b). More recently Jackson & Persson (1995) have done quantum calculations describing the reactive collision near a flat rigid surface, case in which the dynamics can be described with only three degrees of freedom. For the metallic surface, the flat approximation for the surface seems valid because the diffusion barrier is relatively low compared to the chemisorption energy.

In the present work, the corrugation of the graphite surface has been explicitely taken into account. Consequently, a classical and a quasi-classical (QCT) approach have been used. The collision has been analysed from a molecular dynamics (MD) simulation which involves the propagation of classical trajectories in the 12-D phase space. Recently Kratzer (1997) has followed the same theoretical scheme to describe the H_2 formation on a silicon surface Si(001). It is interesting to note that Persson & Jackson (1995a,1995b) have compared their fully-quantum calculations to the QCT method and concluded that the gross features of the dynamics are well described by the QCT method.

Sect. 2 of this paper describes the hamiltonian of the system and the empirical potential model which was used. Sect. 3 presents the computational aspect of the dynamics and the means used to characterize the system. Sect. 4 is devoted to the presentation and the discussion of the results obtained from the MD simulations.

2. Hamiltonian and potential energy surface

2.1. The model

The graphite surface has been modeled by a rigid cluster. Consequently, only 6 degrees of freedom are necessary to describe the reactive collision in the vicinity of the surface. The hamiltonian of the whole system can be written as:

$$H = \sum_{i=1}^{2} \frac{\boldsymbol{p}_i^2}{2m} + V_{int}(\boldsymbol{r}_1, \boldsymbol{r}_2) \qquad (1)$$

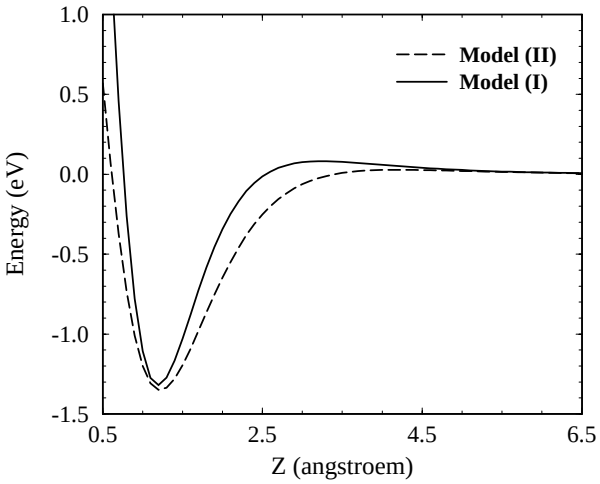

Fig. 1. Plot of the graphite-H interaction potential as a function of the z desorption coordinate. The solid curve and the dashed curve correspond respectively to model (I) and model (II).

where $\boldsymbol{r}_i$ and $\boldsymbol{p}_i$ are respectively the position and the conjugated momentum of the ith H atom; m is the mass of one hydrogen atom.

From this Hamiltonian, the equations of motions of the H atoms near the surface can be easily derived from Hamilton's equations:

$$\frac{d\boldsymbol{p}_i}{dt} = -\frac{\partial H}{\partial \boldsymbol{r}_i} \text{ and } \frac{d\boldsymbol{r}_i}{dt} = \frac{\partial H}{\partial \boldsymbol{p}_i} \qquad \text{for i = 1, 2} \qquad (2)$$

The choice of a rigid surface for this system is justified by the small mass of the hydrogen atom with respect to the carbon one, so that a small energy transfer to the surface (small coupling with the phonons) is expected. A comparison between rigid and non-rigid surface is in progress and will published later.

The crucial point for predicting the reactivity of one H atom with another H atom adsorbed on the graphite surface is the interaction potential. For the purpose of calculation we need a realistic description of the interaction through an empirical potential model. The model potential energy surface (PES) has been built from atom-atom potentials with parameters which naturally depend on the chemical nature of the binding of the involved atoms with the surface. The interaction potential V_{int} can be decomposed as a sum of two terms that are detailed heredown.

Surface-H interaction

The first term ($V_{Surface-H}$) corresponds to the interaction between all the H atoms and the surface. The binding energy of one isolated chemisorbed H atom on graphite has been calculated by different authors using ab-initio procedure (Bennet et al. (1971); Aronowitz & Chang (1985); Klose (1989) and Fromherz et al (1993)). These numerical values are strongly different depending on the methods used by these authors. In this work, we have chosen to reproduce qualitatively the ab-initio results obtained by Fromherz et al. (1993). The

Table 1. Potential parameters for the H-graphite interaction.

	Model (I)	Model (II)
D_0 (eV)	0.665	0.600
β (Å^{-1})	2.60	2.00
r_c (Å)	1.80	1.80
α (Å^{-1})	0.90	0.90
$D_{SH}^{(0)}$ (eV)	41.50	12.25
$D_{SH}^{(\infty)}$ (eV)	2.48	2.48
γ (Å^{-1})	2.60	1.00

interaction potential has been written as:

$$V_{Surface-H} = V_{atom-atom} + V_{rep} \quad (3)$$

The first contribution $V_{atom-atom}$ is calculated from a sum of pairwise atom-atom terms between each of the H atoms and the N_c (= 67) effective centers of forces located at the centers of the benzenic rings. We have:

$$V_{atom-atom} = \sum_{i=1}^{n} \sum_{\alpha=1}^{N_c} D_0 \, [[1 - e^{-\beta(r_{i\alpha} - r_c)}]^2 - 1] \quad (4)$$

As the interaction between the surface and an H_2 molecule or a H atom is strongly different, the progressive evolution from the net chemisorption of H to the much weaker adsorption of H_2 is accounted for by the addition of a purely repulsive (V_{rep}) term whose magnitude depends on the H-H distance by:

$$V_{rep} = \sum_{i=1}^{n} D_i' \, e^{-\alpha z_i} \quad (5)$$

where z_i is the coordinate of the i^{th} H atom along the axis perpendicular to the surface, and D_i' is depending on the H-H distance (d_{HH}) by the following relation:

$$D_i' = D_{SH}^{(\infty)} + (D_{SH}^{(0)} - D_{SH}^{(\infty)}) \exp^{-\gamma d_{HH}}$$

The values of all the parameters used to describe the surface–H interaction are reported in Table 1.

H-H interaction

The second contribution (V_{H-H}) to the total potential energy is the lateral interaction between all the H atoms. A Morse potential has been used to describe this interaction:

$$V_{H-H} = \sum_{i=1}^{n} \sum_{j>i} D_z[[1 - \exp^{-\beta'(r_{ij} - r_e)}]^2 - 1] \quad (6)$$

r_{ij} is the distance between the i^{th} and the j^{th} H atoms. r_e is the equilibrium distance of the diatomic molecule in the gas phase. D_z is the binding energy for the Morse potential. In our model, we assume that the magnitude of D_z depends on the localization of the diatomic with respect to the surface as:

$$D_z = D_{HH}^{(\infty)} + \frac{1}{2}(D_{HH}^{(0)} - D_{HH}^{(\infty)}) \sum_{i=1}^{2} \exp^{-\gamma' z_i} \quad (7)$$

z_i is the z coordinate of the i^{th} H atom and $D_{HH}^{(\infty)}$ the binding energy for the isolated H_2 molecule in the gas phase in its ground electronic state $^1\Sigma_g^+$.

Table 2. Potential parameters for the H-H interaction.

β' (Å^{-1})	1.970
r_e (Å)	0.741
$D_{HH}^{(0)}$ (eV)	0.500
$D_{HH}^{(\infty)}$ (eV)	4.751
γ' (Å^{-1})	2.000

2.2. Characteristic features of the reactive surface

Values of all the $H - H$ potential parameters are reported in Table 2. As noted just before, the potential model has been built in order to reproduce the main characteristics of the H-graphite potential calculated by Fromherz et al. (1993). These authors have found that the binding energy of the most stable configuration was equal to -1.31 eV which corresponds to a weak chemisorption. In this equilibrium structure, the H atom is just located above a carbon atom and the z coordinate is equal to 1.15 Å. In this minimum energy configuration, they have found that graphite surface was locally reconstructed: the carbon atom is attracted to the H atom. This tendency to form a tetrahedron results from the evolution from a sp^2 (graphite) to a sp^3 character.

Concerning the chemisorption of the atomic hydrogen, one only site has been found with the two models described in the previous section. The H atom is on a top position just above a carbon atom. In the potential model (I), the binding energy is equal to $E^{(H)}$ = -1.32 eV and the distance between the H atom and the carbon atom is equal to 1.19 Å. In Fig. 1 is plotted the potential energy curve along the z coordinate for a single H atom. A small activation barrier ($E_b^{(H)}$ = 0.081 eV) appears at z = 3.20 Å. A saddle point between two equivalent top sites appears in the middle of the C-C bond. The height of this barrier for the H diffusion (or migration) is equal to 0.25 eV. The middle of the C-C bond and the center of the ring correspond to saddle points in the PES.

In the case of model (II), the topology of the PES is not strongly modified. In the minimum energy configuration, the H atom is always located just above a carbon atom at a slightly larger value of z (z_e = 1.22 Å). The corresponding energy is equal to $E^{(H)}$ = -1.35 eV. In this second model, the activation barrier along the z coordinate is slightly smaller ($E_b^{(H)}$ =0.028 eV) and at a larger z value ($z_b^{(H)}$ = 4.20 Å). Comparison between the two proposed models for the dependence of the potential along the z coordinate is displayed in Fig. 1. The consequence of the small barrier at large z for the H–graphite potential is that a small activation barrier is present in the entrance channel of the reactive PES. As pointed out by Fromherz et al. (1993) the reality of this small activation barrier has to be confirmed by more refined ab-initio calculations. Indeed very recent ab-initio calculations based on the density functional theory (Jeloaica & Sidis, private communication) have just confirmed its existence.

About the adsorption site for the H_2 molecule, the two models give a minimum energy configuration with the H_2 molecule parallel to the surface. With model (I) the binding energy is

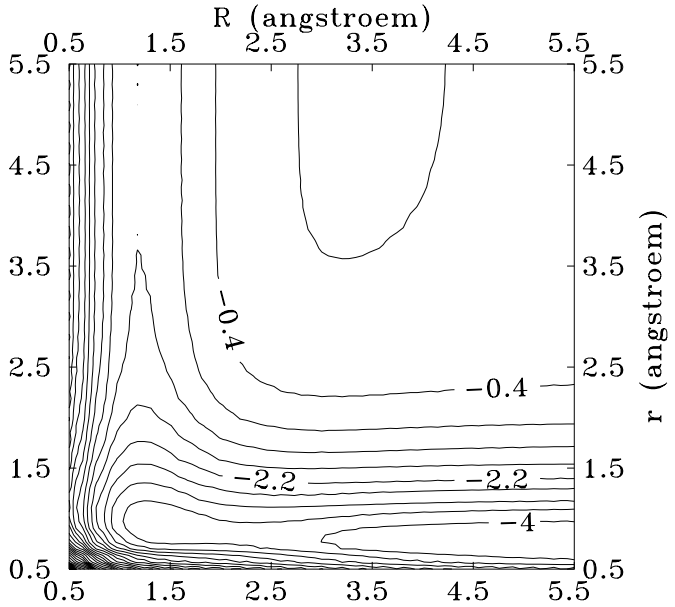

Fig. 2. Contour plot of the reactive PES in a collinear collision for potential model (I). The spacing between contour lines is equal to 0.45 eV.

Table 3. Characteristics of the H-graphite potential energy surface. $z_e^{(H)}$: equilibrium distance of the chemisorbed H from the surface; $E^{(H)}$: binding energy in the chemisorption site; $z_b^{(H)}$: distance of the barrier in the entrance channel from the surface; $E_b^{(H)}$: energy at the top of the barrier.

	Model (I)	Model (II)	Fromherz et al. (1993)
$z_e^{(H)}$ (Å)	1.19	1.22	1.15
$E^{(H)}$ (eV)	-1.32	-1.35	-1.31
$z_b^{(H)}$ (Å)	3.20	4.20	2.35
$E_b^{(H)}$ (eV)	0.081	0.028	0.090

equal to $E^{(H_2)}$ = - 0.112 eV, and slightly smaller $E^{(H_2)}$ = - 0.088 eV in the case of model (II). This is in good agreement with the value proposed by Ross et al. (1964)

(- 0.084 eV), and of the same order of magnitude as the values derived by Mattera et al. (1980) from scattering experiments (-0.052 eV). Unfortunately, to our knowledge, no experimental information is available about the localization of this site with respect to the surface.

Since we are interested in the recombination process it is useful to look at a representation of the total reactive H-Surface-H PES. Fig. 2 is a contour plot of the total PES of model (I) in the collinear approach above a top site, using as reaction coordinates the $H-H$ distance r and the C-H distance R from the chemisorbed H atom to the surface. In this graph an ER process is represented by a trajectory coming from the top at large r and with $R \approx 1.2$ Å and ending at the lower right corner at large R with $r \approx 0.7$ Å. The activation barrier in the entrance channel is too small to be seen in this figure. All the data about the minimum energy configurations for H on graphite with the two potential models have been summarized in Table 3.

3. Dynamical calculations

The equations of motion (Eqs. (2)) for the H atoms have been numerically integrated with an Adams-Moulton fifth order predictor-corrector algorithm. Consequently, a constant energy trajectory was run in the phase space. The time step for this propagation was equal to 0.10 fs. The energy conservation was satisfied to about 10^{-5} for one typical trajectory.

The initial coordinates of the colliding H atom was randomly chosen in a (x,y) square cell of size $2L \times 2L$. Most of the calculations have been made with L = 5 Å. The z coordinate of this atom was initially set at 15 Å, a distance where the interaction between the H atom and the surface was negligible. The initial momentum of this H atom was also randomly chosen to describe a given gas phase equilibrium temperature following a Maxwell-Boltzmann distribution.

In this work, most of the results have been obtained with the direction of the initial momentum normal to the surface. However, to analyse the influence of an initial angular distribution, we have generated some trajectories with the angle between the normal vector and the velocity vector randomly chosen between -$\Delta\alpha$ and + $\Delta\alpha$.

For the other hydrogen atom, two different procedures have been used. The first one, which we call the classical one, consists to prepare the initially chemisorbed H atom on carbon cluster at a given kinetic temperature T_{chem} calculated from the equipartition theorem:

$$T_{chem} = \frac{2\overline{E}_{kin}}{3\ k_b} \tag{8}$$

k_b is the Boltzmann constant and $\overline{E}_{kin}$ corresponds to the time averaged kinetic energy of the chemisorbed atom before the other H atom is in interaction with the surface. T_{chem} has been chosen around 70 K which means that the H adsorbed atom was prepared near its equilibrium configuration with only a very small amount of vibrational energy. In this approach the zero-point energy was not considered.

The second procedure corresponds to a quasi-classical trajectory (QCT) in which the zero-point energy (ZPE) of the H atom on the graphite surface is taken into account by a semi-classical method based on the Ehrenfest adiabatic theorem. We built a separable harmonic potential $H_0(x, P_x, y, P_y, z, P_z)$ defined by:

$$H_0 = \frac{\boldsymbol{P}^2}{2m} + \frac{1}{2}\left[k_x(x-x_e)^2 + k_y(y-y_e)^2 + k_z(z-z_e)^2\right] \tag{9}$$

x_e, y_e and z_e are the cartesian coordinates of the equilibrium configuration in the *"real" H*–graphite potential. In this harmonic separable hamiltonian, one can select trajectories which satisfy the semi-classical quantization by:

$$\begin{cases} x &= \sqrt{\frac{(v_x+1/2)h}{\pi m\omega_x}}\ \sin\varphi_x \\ P_x &= \sqrt{\frac{m\omega_x(v_x+1/2)h}{\pi}}\ \cos\varphi_x \end{cases} \tag{10}$$

φ_x is randomly chosen in the [O;2π] interval. $\omega_x (=\sqrt{\frac{k_x}{m}})$ is the pulsation.

The same relations are to be considered for y, P_y, z and P_z. Consequently for a set of vibrational quantum numbers (v_x, v_y, v_z), we can select trajectories in the phase space corresponding to the H_0 hamiltonian. To transform the harmonic hamiltonian into the *"real"* hamiltonian, we built a time-dependent hamiltonian $H(t)$ defined as:

$$H(t) = \frac{\boldsymbol{P}^2}{2m} + V_h(x,y,z) + g(t)[V_r(x,y,z) - V_h(x,y,z)] \quad (11)$$

$V_h(x,y,z)$ is the harmonic potential defined previously and $V_r(x,y,z)$ is the *"real"* potential. g(t) is a slowly varying time dependent function, defined for t $\in$[0;T_a], by:

$$g(t) = \frac{t}{T_a} - \frac{\sin(2\pi\frac{t}{T_a})}{2\pi} \quad (12)$$

In this work, T_a was taken equal to 1 ps. During the adiabatic switching, quantum numbers v_x, v_y and v_z are conserved if the transformation is a slow enough process (T_a has to be larger than $\approx$ 100 $\times$ characteristic vibrational period of the system). The final coordinates and associated momenta satisfy the semi-classical quantization and then are associated to a set of vibrational quantum numbers in the *"real"* hamiltonian. They are taken as initial coordinates and momenta for the collisional trajectories.

The maximum duration of one collisional trajectory was equal to 12 ps. During this microcanonical trajectory, if the z coordinate of one H atom was found greater than 15 Å, this atom was considered as desorbed. A distance criterion was then used to test if a H_2 molecule had been formed: if the distance between the two H atoms was smaller than 2.0 Å, a molecule was considered as desorbed to the gas phase.

If this was the case, the tranlational, rotational and vibrational energies of the H_2 molecules were evaluated. The translational energy is given by $E_{tr} = \frac{\boldsymbol{P}^2_{com}}{2M_{H_2}}$ in which $\boldsymbol{P}_{com}$ is the linear momentum of the H_2 molecule center of mass and M_{H_2} is the mass of the diatomic molecule. The vibrational part is calculated as $E_{vib} = \frac{P_r^2}{2\mu}$, and the rotational contribution is calculated by $E_{rot} = \frac{\boldsymbol{J}^2}{2\mu r^2}$. $\boldsymbol{J}$ is the angular momentum of the H_2 diatomic molecule and μ its reduced mass.

A semi-classical vibrational number v was calculated from the semi-classical quantization of the action integral:

$$(v+\frac{1}{2})h = \oint P_r dr = \oint \sqrt{2m(E_{int} - V(r) - \frac{J^2}{2\mu r^2})}\, dr \quad (13)$$

$V(r)$ is the internuclear potential of the H_2 isolated molecule in its ground electronic state. E_{int} is the rovibrational energy of the molecule and h is the Planck's constant.

For a given set of parameters ($\Delta\alpha$, $\overline{E}_{coll}$, T_{chem} or (v_x, v_y, v_z)), 2000-8000 trajectories have been run to obtain statistically significant results.

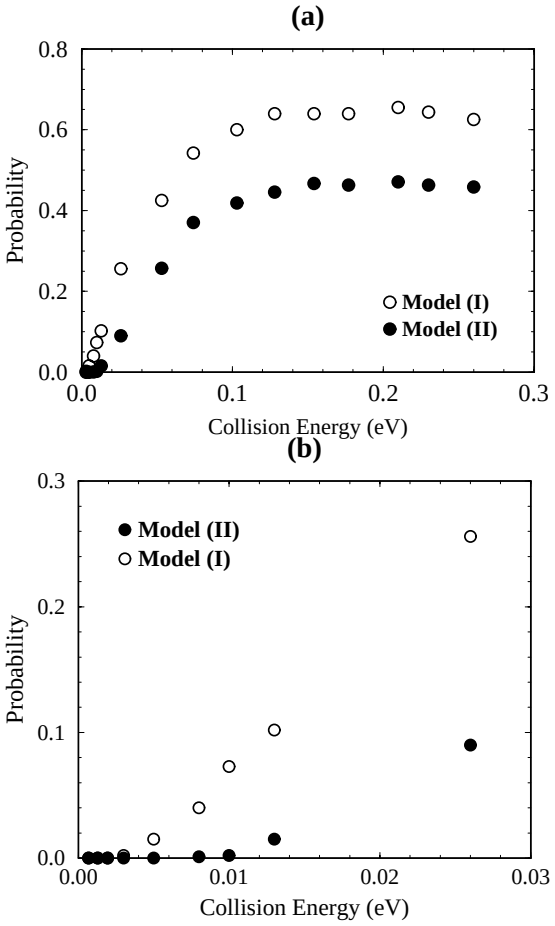

Fig. 3a and b. Plot of the H_2 recombination probability versus the collision energy ($\overline{E}_{coll}$) obtained in the case of a single H adatom in a cell of 100 Å^2, with the two potential models; **a** corresponds to the full energy range; **b** is a zoom in the low energy range.

4. Dynamical results and discussion

4.1. Rate of recombination of the H_2 molecule

4.1.1. Results of the simulation

The H_2 recombination probability during the collision is plotted as a function of the collision energy ($\overline{E}_{coll}$) in Fig. 3 (the direction of the velocity of the incoming H atom was taken perpendicular to the rigid surface, and L = 5 Å). For the two potential models studied, similar behaviour was obtained. A clear increase of the probability with the collision energy appears from Fig. 3a. At low collision energy ($\overline{E}_{coll} < E_{min}$), no hydrogen molecule is formed along the classical trajectories in the phase space, the incoming H atom being reflected back to the gas phase at relatively large z value. The values of E_{min} are slightly dependent on the potential model. We obtained $E_{min} \approx 3\ meV$ for model (I) and $E_{min} \approx 10\ meV$ for model (II) (see Fig. 3b). The effective activation barrier for reactivity is then slightly higher in the case of model (II) although that the H–graphite barrier is lower. This difference is the consequence of the localization of the barrier. Indeed the activation barrier is found at a smaller value of z for model (I) so that the $H - H$

Table 4. Comparison of the results obtained from the CT and QCT methods. P_{H_2} is the recombination probability; $\overline{E}_{tr}$, $\overline{E}_{rot}$, $\overline{E}_{vib}$ are the averaged energies in various degrees of freedom of the nascent H_2. Calculations were made with potential model (I). All energies are given in eV.

$\overline{E}_{coll}$	0.013	0.013	0.026	0.026	0.132	0.132
Method	CT	QCT	CT	QCT	CT	QCT
P_{H_2}	0.11	0.13	0.25	0.27	0.65	0.66
$\overline{E}_{tr}$	1.66	1.75	1.67	1.77	1.80	1.87
$\overline{E}_{rot}$	0.53	0.74	0.61	0.74	0.71	0.78
$\overline{E}_{vib}$	1.29	1.20	1.22	1.20	1.08	1.15

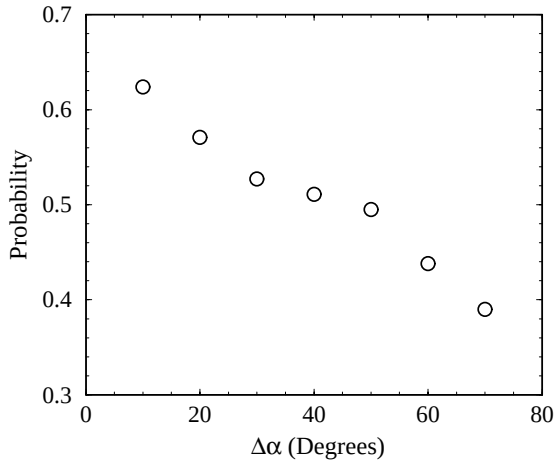

Fig. 4. Plot of the H_2 recombination probability as a function of the maximum angle $\Delta\alpha$ (see text) of the initial velocity from the normal to the surface at $\overline{E}_{coll}$ = 0.132 eV in the case of potential model (I) from a set of 4000 trajectories.

attractive interaction is then larger than in the case of model (II). Consequently the global barrier in the entrance channel is lower for potential model (I) as compared to model (II).

From a classical point of view, no trajectory can go through this potential barrier. However a quantum description of this reactive pathway could give a non-zero probability for the H atom to tunnel through this barrier. Consequently one could presume that the rate of H_2 formation at low collision energy in the classical approach is certainly slightly lower than in a complete quantum treatment.

When $\overline{E}_{coll}$ becomes larger than E_{min}, the H_2 formation is now energetically allowed for an increasing number of trajectories. Consequently the efficiency of the formation process increases as a function of $\overline{E}_{coll}$. The probability to form a molecule reaches a maximum at $\overline{E}_{coll} \approx 0.15\ eV$. At this energy, almost 65 % of the trajectories are reactive with model (I) and ≈ 45 % with model (II). The recombination is then highly efficient in this range of energy. When the collision energy becomes larger than ≈ 0.15 eV, the efficiency of the recombination process remains almost constant.

Up to now, we have only considered the situation in which the initial velocity of the atomic hydrogen is normal to the graphite surface. In Fig. 4, the formation probability has been plotted as a function of $\Delta\alpha$ at a collision energy $\overline{E}_{coll}$ = 0.132 eV. When $\Delta\alpha$ increases, a net lowering of the recombination rate appears. This reflects the decrease of the normal component of the incoming H linear momentum. Consequently, when $\Delta\alpha$ decreases, more and more atoms are reflected on the activation barrier along the z coordinate. If only the normal component of the linear momentum of the incoming particule is to consider in the reactive collision, we expect to find that the recombination probability at $\overline{E}_{coll} = E_0$ for $\Delta\alpha = 90^0$ will be equal to the recombination probability at $\overline{E}_{coll} = E_0/3$ for $\Delta\alpha = 0^0$. In Fig. 4, if we extrapolate the curve up to $\Delta\alpha = 90^0$, we obtain $P_{H_2} \approx 0.36$ with E_0 = 0.132 eV. This value is in very good agreement with that obtained at $\Delta\alpha = 0^0$ at the collision energy $E_0/3$ = 0.044 eV, i.e. $P_{H_2} \approx 0.38$ (see Fig. 3a). Consequently, if we want to transform the collision energy into a gas phase temperature T_g, we have to use the relationship $\overline{E}_{coll} = \frac{1}{2}k_bT_g$ with $\Delta\alpha = 0^0$. Consequently, the gas temperatures, associated to the appearance of the recombination process, are respectively 70 K and 230 K for the potential models (I) and (II).

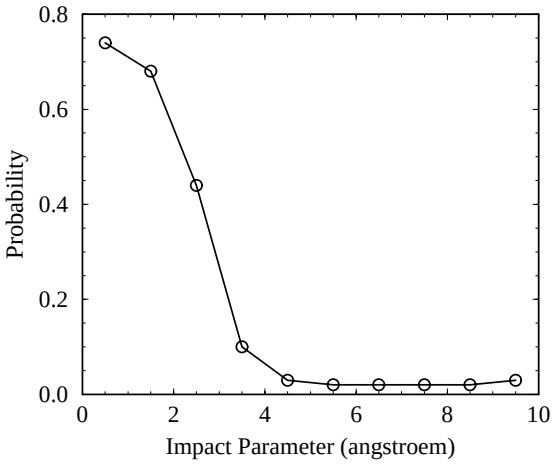

Fig. 5. Plot of the H_2 recombination probability as a function of the impact parameter b at $\overline{E}_{coll}$ = 0.026 eV. These results have been obtained with potential model (I) from a set of 8000 independent trajectories with L = 5 Å.

As said in the previous section, the H adsorbed atom was prepared at a given equilibrium temperature T_{chem}. All the results shown up to now have been obtained at $T_{chem} \approx 70$ K. The recombination rate has also been calculated for increasing values of T_{chem} in the 10-250 K range. It was found that the formation rate was almost unsensitive to the initial vibrational energy of the adsorbed H atom.

In Table 4, the formation probability obtained from both CT and QCT calculations at three values of the collision energies are reported. The sensitivity of the process efficiency with respect to the method is weak. The formation probability was found slightly larger in the QCT calculation than in the CT calculation, which can be explained by the zero-point energy (≈ 0.23 eV) deposited in the H-graphite system at the beginning of each trajectory. It is clear again that the increase of the initial H-graphite vibrational energy does not affect much the efficiency of the process. On the contrary, a 0.20 eV increment in the collision energy completely affects the formation probability. This

Table 5. Comparison of the total cross-section (σ_{tot}) and the Eley-Rideal cross-section (σ_{ER}) for potential model (I). The two cross-sections, calculated with L = 5 Å, are defined in the text.

$\overline{E}_{coll}$ (eV)	0.013	0.026	0.132
σ_{tot} (Å^2)	7.6	19.0	61.9
σ_{ER} (Å^2)	7.6	17.6	43.0

strong difference reveals that the process is mainly governed by an activation barrier in the entrance channel.

It is now of interest to analyse the recombination probability as a function of the impact parameter b. It appears that a large proportion of molecules are formed when the impact parameter b is less than 2 Å. For each set of trajectories, we have calculated the opacity function $P(b)$, defined as the ratio of the number of reactive trajectories to the total number of trajectories which are characterized by an impact parameter in the interval $[b; b + db[$. The opacity function derived from 8000 trajectories at $\overline{E}_{coll}$ = 0.026 eV in the case of model (I) is plotted in Fig. 5. From the opacity function, the cross-section can be easily derived as:

$$\sigma = 2\pi \int_0^\infty P(b)\, b\, db \tag{14}$$

The values of σ, reported in Table 5, are relatively large. However we have to keep in mind that this cross-section reflects not only the direct ER process between the incoming H atom and one isolated hydrogen atom on an infinite surface but also the indirect process. This last one involves trajectories during which the incoming H atom is trapped and migrates on the surface until it reacts with one of the other adsorbed H atoms. In the simulation this process is taken into account thanks to the periodic boundary conditions in the (x,y) plane. To estimate the relative importance of such a process, a process was considered as indirect if the incoming H atom, isolated from the other one, left the cell during the trajectory. In Table 5, the cross-section associated to the direct ER process (σ_{ER}) has been tabulated for three collision energies. It clearly appears that the ratio between direct and indirect processes is strongly dependent on the collision energy. In the low energy regime, all the recombination events are direct. The lower is the collision energy, the more the incoming H atoms are sensitive to the adsorbed H atom which acts as an attractor. This explains why the indirect process becomes negligible when the collision energy decreases. On the other hand, at $\overline{E}_{coll}$ = 0.132 eV, a substantial proportion of indirect processes are observed. In this range of collision energy, the linear momentum orientation transfer is dominated by the surface corrugation rather than by the influence of the other H atom and the proportion of indirect trajectories increases. We have also analysed the probability to form H_2 in such indirect trajectories: it was found equal to 66 % at $\overline{E}_{coll}$ = 0.026 eV and 55 % at $\overline{E}_{coll}$ = 0.132 eV respectively. This lowering of the efficiency of the recombination process as a function of the incident kinetic energy corroborates that the migrating H atoms are less and less sensitive to the adsorbed H atom when $\overline{E}_{coll}$ becomes larger and larger. This explains the slight decrease of the total recombination efficiency as visible in Fig. 3a.

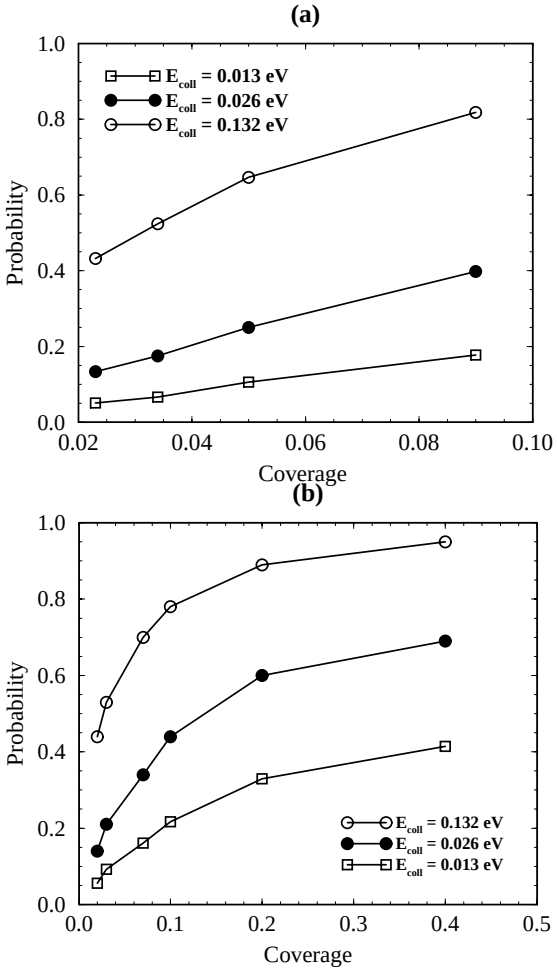

Fig. 6a and b. Plot of the H_2 recombination probability versus the coverage (η) at three different collision energies with potential model (I). **a** Results obtained for η <0.1 by changing the area of the cell in classical trajectories. **b** Results obtained for larger coverage (up to 0.4) from the distribution of impact parameters and the data in Fig. 5.

All the results discussed below have been obtained with the area of the square cell equal to 100 Å^2. As the cross-sections are certainly dependent on the density of adsorbed H atoms per unit area, or equivalently on the coverage η (in units of a monolayer, *i.e.* when all the top sites are occupied), we have analysed the evolution of the formation probability as a function of η by changing the area of the cell (a cell of 100 Å^2 corresponds to $\eta \approx 0.05$). This procedure allowed to obtain informations in the range of low coverage ($\eta < 0.1$). These results have been reported in Fig. 6a for three different collision energies. It appears that, for the 2 lowest values of $\overline{E}_{coll}$, the recombination efficiency is linear with respect to the coverage. On the other hand a slight saturation of the recombination probability appears at $\eta \approx 0.09$ at $\overline{E}_{coll}$ = 0.132 eV. In fact the non-linearity appears for a critical H density $\rho_H^{(c)} = \frac{1}{\pi\, b_{max}^2}$ in which b_{max} corresponds to the characteristic value of the impact parameter for which the opacity function vanishes. As b_{max} increases as a function of the collision energy, it explains that the non-linearity is observed in the MD calculations for the lowest $\overline{E}_{coll}$.

To obtain information relative to larger coverage, an alternative procedure has been used. The opacity functions P(b) have been calculated as explained above for different collision energies. For a given coverage (η), the distribution of the impact parameter ($g^{(\eta)}$(b)) was calculated from a set of randomly chosen initial conditions in a cell whose size is adapted to the coverage. From P(b) and $g^{(\eta)}$(b), the recombination probability was easily deduced from:

$$P_{H_2}(\eta; \overline{E}_{coll}) = \int_O^\infty g^{(\eta)}(b)\ P(b)\ db \tag{15}$$

The $P_{H_2}(\eta; \overline{E}_{coll})$ function is plotted in Fig. 6b for the same three collision energies up to $\eta \approx 0.4$.

4.1.2. Discussion of the astrophysical consequences

This H_2 recombination probability at given coverage $P_{H_2}(\eta; \overline{E}_{coll})$ is crucial to extract useful information for astrophysics. Indeed, the most important quantity for interstellar hydrogen chemistry is the H_2 formation rate (in $cm^{-3}.s^{-1}$) which is given by:

$$R_{H_2} = n_H\ \overline{v}_H\ n_g\ \sigma_g\ P_{H_2}(\eta; \overline{E}_{coll}) \tag{16}$$

In this last expression, n_H and $\overline{v}_H$ corresponds respectively to the atomic hydrogen density in the gas phase and to the mean velocity of these H atoms (which is related to the gas temperature if this phase is considered to be at thermodynamical equilibrium in the ISM). n_g and σ_g are respectively the dust grain density in the ISM and the mean surface offered by the average grain (depending in particular on the geometry of the dust particle).

In standard astrophysical models of H_2 formation in the ISM, such as the one proposed by Hollenbach & Salpeter (1970,1971), the rate is estimated within the hypothesis of a very high recombination probability (≈ 0.3), supposed to be the product of the sticking probability S_H by a factor γ (close to 1) implicitely assumed to account for the efficiency of the LH mechanism, independently of any explicit reference to the amount of adsorbed hydrogen as measured by the coverage. Indeed this formulation is equivalent to consider that the reaction probability is never limited by the diffusion of the adatoms. This assumption would need a specific study in order to check its validity in the low T_d range. We estimate nonetheless that diffusion coefficient large enough to permit an average diffusion velocity of the order of 1 Å/year or more is necessary for the reactivity to be dominated by the LH mechanism. Note that these diffusion processes are expected to be very sensitive to the chemical composition and physical structure of the grains surfaces.

On the contrary if we neglect thermal desorption and the LH process, which will tends to be valid in dense and cold regions of the ISM, the steady-state coverage, η_e, resulting from the equilibrium between sticking and H_2 formation by the ER mechanism will result from:

$$P_s(\eta; \overline{E}_{coll}) = P_{H_2}(\eta; \overline{E}_{coll}) \tag{17}$$

$P_s(\eta; \overline{E}_{coll})$ corresponds to the sticking probability for the H atom impinging onto the grain. It depends parametrically on the coverage η and on the mean collision energy. With the very simple assumption that this sticking probability is proportionnal to the number of available sites, we have $P_s(\eta; \overline{E}_{coll}) = (1 - \eta) \times P_s(\eta = 0; \overline{E}_{coll})$. The reaction probability has been found to be an increasing function of the coverage (see Fig. 6). The two probability functions will then cross over at the steady state value η_e of the coverage. assuming $P_s(\eta = 0; \overline{E}_{coll}) = \frac{1}{2}$ as an order of magnitude, one obtains η_e = 0.3 at $\overline{E}_{coll}$ = 0.013 eV (i.e. $T_g \approx 300$ K). The corresponding recombination probability is ≈ 0.35, which is very much the same as the commonly admitted value (Hollenbach & Salpeter 1970,1971, Jura 1975). The average gas temperature in the ISM is smaller than 300 K but the above value can be reached in shocked regions or heated regions, such as photon dominated regions where H_2 is more readily observed. As a matter of fact the grain to gas relative velocity is the quantity which governs the value of $\overline{E}_{coll}$ and it may be affected by grain acceleration and/or friction in stellar winds. Finally one should keep in mind that these numbers depend rather crucially of physical quantities not accurately known such as the barrier in the entrance channel.

4.2. Distribution of excess energy in the nascent H_2 molecule

Besides the direct astrophysical consequences, the interest to examine the distribution of excess energy in the nascent H_2 molecules has been strengthened by the recent experimental results obtained by Gough et al. (1996) on the internal states distribution of H_2 molecules desorbed from carbonaceous surfaces exposed to thermal H atoms. H_2 molecules in highly excited vibrational states up to v = 7 were observed. On the other hand no significant rotational excitation was observed. This experimental study has been realized for different values of the surface temperature.

In the MD simulations, we have been interested in the repartition of the excess energy available in the chemical reaction induced in the vicinity of the graphite surface among the various degrees of freedom of the product, *i.e.* H_2. With the two potential models used in this work, the reaction is highly exoenergetic (ΔE $\approx 3.4\ eV$). In Fig. 7, the ensemble averages of the translational kinetic energy, rotational energy and vibrational energy of the newly formed H_2 molecules have been plotted for 9 different values of $\overline{E}_{coll}$ in the case of model (I). As it can be seen in this plot, the partitioning of the energy in the different degrees of freedom is almost independent of the collision energy. This result can be easily understood by noting that the increase of the collision energy represents only a small amount with respect to the reaction exothermicity. A precise analysis of the results given in Table 4 shows that the translational and rotational energies of H_2 increase slowly as a function of the collision energy. On the other hand the vibrational energy tends to decrease slightly. But the ordering $\overline{E}_{tr} > \overline{E}_{vib} > \overline{E}_{rot}$ remains unchanged.

A large amount of the excess energy ($\approx 50\,\%$) is then devoted to the overall translation energy of the H_2 molecule. This large

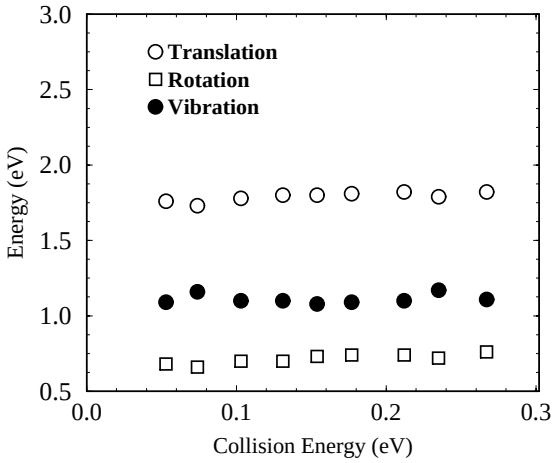

Fig. 7. Distribution of excess energy in the reaction among various degrees of freedom: ensemble averages of translational, rotational and vibrational energies of the newly formed H_2 molecules as a function of the collision energy of the impinging H atom. These results have been obtained with potential model (I).

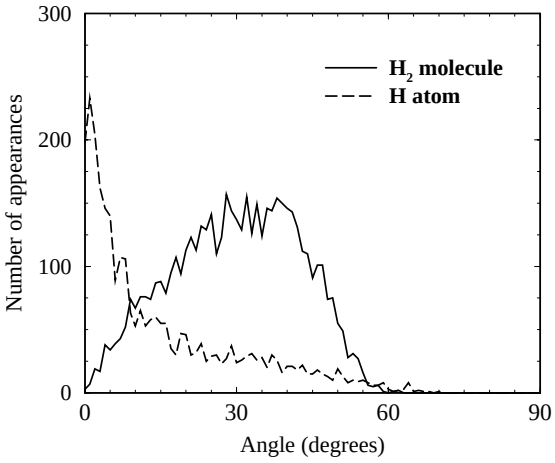

Fig. 8. Angular distribution of the scattered H atoms and of the newly formed H_2 molecules at $\overline{E}_{coll}$ = 0.132 eV with potential model (I). Angles are referred to the surface normal.

kinetic energy associated to the recoil of the H_2 molecules following the recombination mechanism at the gas-solid interface could have important consequences for the physics and chemistry of the ISM. Indeed these newly formed H_2 molecules could induce an efficient heating of the interstellar gas.

The direction of the desorbed H_2 molecule following the collision has also been analysed. This information could be useful for experiments in which the detection of the desorbed H_2 molecules could be angularly resolved. The angular distribution of the desorbed H_2 molecules is diplayed in Fig. 8 (solid line). It presents a maximum at $\theta \approx 35$ degrees, and is almost unsensitive to the initial collision energy. The angular distribution for the back-scattered H atom (dashed curve) is maximum at $\theta = 0$ but is broadened due to the surface corrugation.

The rotational degrees of freedom are the less favored. Only $\approx 19\,\%$ of the excess energy is going into the rotation of the diatomic molecule. The distribution of the rotational populations

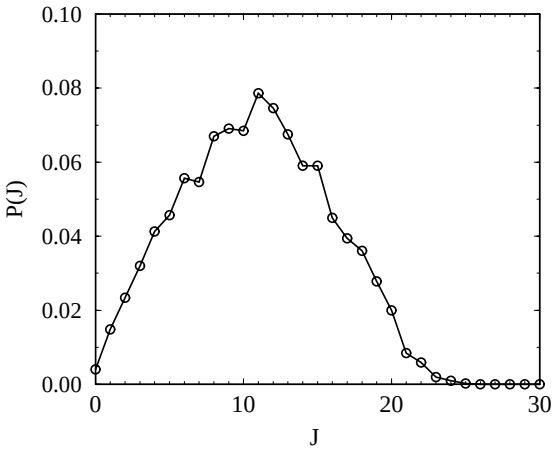

Fig. 9. Rotational angular momentum distribution of the nascent H_2 molecules, P(J), in a QCT calculation at $\overline{E}_{coll}$ = 0.132 eV. J is expressed in $\hbar$ units.

in the nascent H_2 has been obtained from the analysis of the final angular momentum of the diatomics, J. It is plotted in Fig. 9. The mean value of J is $< J > \approx 10$ which corresponds to a mean rotational energy $\overline{E}_{rot} \approx 0.70\,eV$. The broad distribution of the angular momentum is in fact the signature of the anti-correlation between translational and internal energies for the desorbed molecules. Since the simulation is classical, no information about the ortho/para population can be extracted. We can only note that, in the work of Persson & Jackson (1995b), quantum distributions P(J) were generally well reproduced by the QCT simulations. Such a low rotational excitation is consistent with experimental observations by Gough et al. (1996).

We have analysed the possible alignment of the angular momentum of the H_2 desorbed molecule to obtain dynamical information on the formation process. Such alignment effects of the desorbed molecules could be experimentally analysed from the spectroscopy of the H_2 molecules with polarized laser beams. An alignment effect in the thermal desorption of H_2 from a palladium surface has been recently observed (Wetzig et al. 1996) in this way.

The distribution of J_z/J for all the trajectories, and also for the selected direct collisions trajectories, has been analysed. These plots (not shown here) display a maximum around zero which means that the angular momentum orientation is favored in the plane parallel to the graphite surface. Surprisingly, the two distributions (direct and total) are almost the same. It indicates that the desorption induced by a hot migrating atom produces almost the same distribution that a direct ER process. In fact, analysis of the direct trajectories reveals that, after the direct harpooning of the incoming H atom, the H_2 molecule may migrate for some time on the surface before being desorbed. This explains why there is no real difference between the two distributions. If we reject these trajectories (i.e. considering only trajectories involving direct formation and direct desorption), the distribution of J_z/J exhibit as more pronounced peak around zero, as expected. For these latter trajectories, we have plotted in Fig. 10 the correlation between J_x/J and J_y/J. A

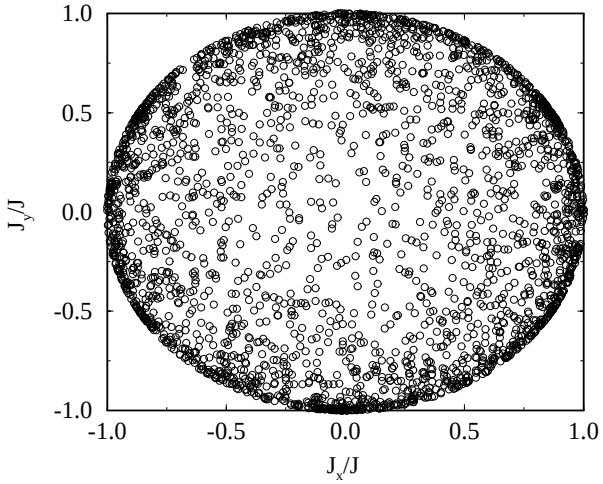

Fig. 10. Plot of the (J_x/J,J_y/J) correlation for the newly formed H_2 molecules. This distribution has been obtained at $\overline{E}_{coll}$ = 0.195 eV with potential model (I) from a set of 8000 trajectories.

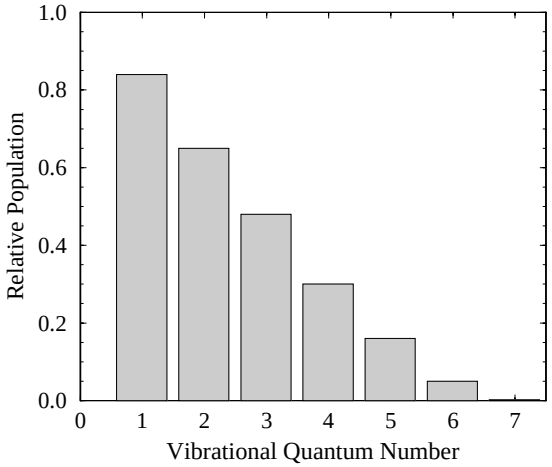

Fig. 11. Vibrational population distribution of the newly formed H_2 molecules, relative to the v=0 population. $\overline{E}_{coll}$ = 0.132 eV, potential model (I), averaged over a set of 8000 trajectories.

clear maximum appears when $(\frac{J_x}{J})^2+(\frac{J_y}{J})^2 \approx 1$, corresponding to trajectories with $J_z \approx 0$. This difference then demonstrates that trajectories involving atomic or molecular migrations tend to be associated to helicopter-like motion in which the angular momentum is along the z direction. A more detailed analysis of the J_x/J and J_y/J distributions also reveals preferential directions peaks which can be correlated to the topology of the graphite-H PES.

About 31 % of the excess energy is transfered into vibrational excitation. The relative population distribution $\frac{N(v)}{N(0)}$ in successive vibrational states obtained at $\overline{E}_{coll}$ = 0.132 eV is shown in Fig. 11. From this set of 8000 trajectories, we observe high vibrational excitations up to v = 6, which is in quite good agreement with the experimental work of Gough et al. (1996) where a vibrational population up to v = 7 has been observed. The calculated vibrational distribution does not exhibit population inversion, nor is characteristics of a thermal distribution which could be the case in a LH process.

However the experimental vibrational distribution reported by Gough et al. (1996) is strongly different from the present prediction. In particular, they found that most of the molecules are formed in the ground vibrational state. They have estimated that the ratio $\frac{N(v=1)}{N(v=0)}$ is less than 0.13. In the calculation presented here, we have found $\frac{N(v=1)}{N(v=0)}$ =0.84. This disagreement call for some comments, since there are many reasons for which calculations and measurements can give different results.

First of all, as said by Gough et al. (1996), a large fraction of the newly formed H_2 molecules may collide many times with the surface before being detected due to the configuration of the experimental set-up. If this is the case, these collisions obviously induce a de-excitation of the diatomics which will alter the measured vibrational distribution. On the other hand it is not clear at all that the microscopic mechanism which mainly induce H_2 desorption in the experiment is the ER mechanism. It may be partly or largely affected by the LH process. Another uncertainty resides in the parametrization of the interaction potential used in the present work, which may not perfectly represent the reactive zone. If we analyse the energy partitionning obtained with potential model (II), the translational contribution is again the most important (41 %) but is however slightly smaller than with the first parametrization. On the other hand, the vibrational contribution (38 %) is now almost equal to the translational one, with a maximum for v = 1. The rotational contribution (21 %) is almost unchanged with respect to model (I). These three contributions are again almost unsensitive to the collision energy over the whole range in which the reactive process has been studied. In summary, potential model (II) tends to increase the vibrational contribution with respect to the translational one.

Table 6. The value of the inelasticity parameter Q (see Eq. (18)) for different collision energies within the CT approach. These results have been obtained with potential model (I). All the energies are given in eV.

$\overline{E}_{coll}$	0.013	0.026	0.132	0.195	0.262
$\overline{E}_{coll}^{(diff)}$	0.012	0.020	0.110	0.195	0.293
Q	0.000	0.000	0.025	0.032	0.039
$N_{mig}^{(indirect)}$	0	0	4	6	20
$N_{mig}^{(direct)}$	0	0	0	5	16

An other possibility could be that a large part of the excess energy is transferred to the excitation of the solid thanks to the coupling with the phonon modes. However preliminary MD results using a non rigid surface model show that this energy transfer is not really efficient in this range of collision energy. Finally a point of major importance is the difference in the structure of the carbonaceous surface involved in the experiment with respect to the perfect graphite surface used in the calculation.

The above discussion concerned the energy distribution obtained from the CT calculations. In Table 4, we present the comparison between the CT and QCT methods. In the QCT calculation, the total energy (translational + internal energies) are larger than in the CT calculation due to the ZPE involved

in the simulation. At high collision energy ($\overline{E}_{coll}$ = 0.132 eV), this excess energy is equally shared by translation, vibration and rotation. On the other hand, at low energy, the ZPE seems to be preferentially transferred to the translational and rotational degrees of freedom. As a counterpart the mean vibrational energy slightly decreases with respect to the CT calculation. Indeed increasing $\overline{E}_{coll}$ or the initial adsorption energy induces the same effect (relative increase of $\overline{E}_{rot}, \overline{E}_{trans}$ and decrease of $\overline{E}_{vib}$). This shows that the energy distribution is mainly governed by the transition state region corresponding to the H_2 molecule adsorbed on the surface.

4.3. Energy transfer in the non reactive trajectories

We turn now to the analysis of the non reactive trajectories during which the incoming H atoms are back-scattered. We defined a parameter Q which characterizes the degree of inelasticity of the collision:

$$Q = \frac{\overline{E}_i^{(nr)} - \overline{E}_f^{(nr)}}{\overline{E}_i^{(nr)}} \tag{18}$$

$\overline{E}_i^{(nr)}$ and $\overline{E}_f^{(nr)}$ are respectively the mean values of the initial and final collision energy of the H atoms after the scattering, the averages being calculated over the subset of trajectories which are non reactive only. As the surface is considered as rigid, the value of Q reflects in fact the energy transfer between the two H atoms. The values of Q have been reported in Table 6 at five different collision energies for the CT calculations. In the low collision energy regime, the collision appears as elastic (Q = 0). The incoming particle is reflected at a large z value and the energy transfer between the hydrogen atoms is not efficient. At intermediate collision energy ($\overline{E}_{coll} \approx 0.05\ eV$), the incoming H atom can come close to the surface and consequently can begin to efficiently exchange energy with the other particle. At $\overline{E}_{coll}$ =0.132 eV, Q is equal to 0.025. At this collisional energy, analysis of the trajectories reveals that some H-impact induced migration of the previously chemisorbed atom on the surface appears. It means that an energy transfer of about 0.25 eV (energy of the diffusion barrier) becomes possible. For example, at $\overline{E}_{coll}$ = 0.262 eV, 8000 trajectories have been run. 2704 trajectories were found non-reactive and 36 trajectories have induced an atomic migration. These diffusing H atoms can play an important role in the reactivity process because, following the first H impact, adsorbed atoms can migrate and thus possibly react with other chemisorbed H atoms to also induce a H_2 desorption. In Fig. 12, we have reported the final (x,y) positions of the adsorbed H atom (filled circles) at the end of each trajectory involving the back-scattering of H. At the beginning of the trajectories, the initial position of the adsorbed atom was around (x=1.4 Å;y=0). The carbon atoms (open circles) are also drawn in this picture to put into evidence that the induced migrations appear along the C-C bonds. An analysis of the trajectories reveal that the induced migrations are almost equally generated by direct ($N_{mig}^{(direct)}$) and indirect ($N_{mig}^{(indirect)}$) collisions (see Table 6). This induced migration has been recently observed by Eilmsteiner et al. (1996) in experiments where the desorption of the D_2 molecule was detected following the impact of H on a deuterated Ni(100) surface.

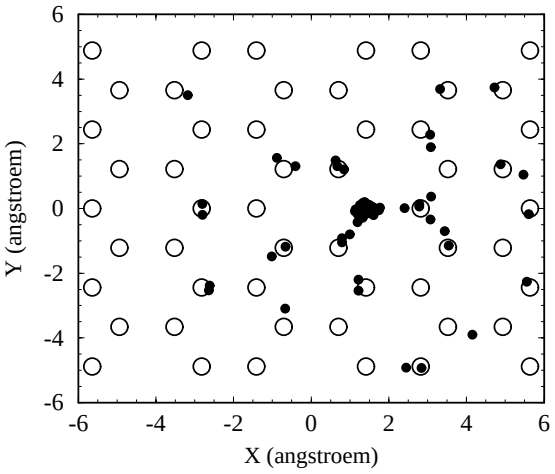

Fig. 12. Final (x,y) in-plane localization of the H adsorbed atom in the non reactive trajectories, obtained at $\overline{E}_{coll}$ = 0.262 eV with potential model (I) from a set of 8000 trajectories. Each open circle represents a carbon atom.

5. Conclusion

For the first time, a complete molecular dynamics simulation has been done to understand the catalytic formation of molecular hydrogen on a graphite surface from a microscopic approach. With the empirical potential model used, it appears that the recombination process favours the formation of highly vibrationally excited molecules with a large translational kinetic energy. The formation efficiency by collision is found as large as 0.5 in the range of 0.1 eV collision energy. As a result of the effect of a small activation barrier in the entrance channel, the onset of the reactivity occurs at around 100 K depending on the potential model. The simulations have revealed the role of both direct and indirect processes, whose relative efficiencies depend primarily on the collision energy and on the surface coverage. The corrugation of the graphite surface plays an important role in the appearance of indirect trajectories because it allows an efficient transfer from normal to tangential components of the incoming H atom linear momentum. An alignment of the rotational angular momentum of the H_2 molecule has been also characterized which seems independent of the nature (direct or indirect) of the collision. Inclusion of the zero-point energy using a semi-classical approach does not alter the results on the formation rate. Its only effect is a slight increase of the mean energy in the translation, rotation and vibration of the newly formed molecules.

Some important astrophysical consequences are outstanding from this study: in particular the possibility to heat the interstellar gas by the recoil energy of the newly formed H_2 molecules, and the hope that the vibrational excitation resulting from this catalytic process becomes a route to recognize regions of formation in space through observations like the vibrational emission

of the H_2 molecule. In order to progress in that direction, refinements of the theoretical approach are necessary, together with confrontation with experiments. On the theoretical side, the first need is the improvement of the interaction, since these phenomena are expected to be strongly dependent on the potential energy surface. We are indeed working now on calculations of the reactive potential energy surface in the framework of the density functional theory. On the experimental point of view detailed dynamical behaviours revealed by the theoretical study, such as of course kinetic energy release and vibrational distribution but also angular distribution and alignment effects, would provide severe tests of the physical reality.

Furher aspects, of direct astrophysical relevance, of the H_2 recombination process which are planned to be studied theoretically in the near future include deuteration effects (important also for experimental reasons), the sticking probability on a non rigid surface, and the Langmuir-Hinshelwood mechanism in which migration of H atoms on the surface dominates the dynamics. The ortho versus para distribution can also be reached through a quantum mechanical treatment. It would allow, through a full astrophysical modelling, to explore in detail the role of physical conditions such as the grain temperature T_d, the gas temperature T_g, the density of the gas n_H, the density of grains n_g and size distribution, as well as grain velocities and interstellar radiation field.

Acknowledgements. This work was supported by the CNRS program "Physique et Chimie du Milieu Interstellaire".

References

Aronowitz S., Chang S., 1985, ApJ 293, 243
Bennet A.J., McCarroll B., Messmer R.P., 1971, Surf. Sci. 24, 191
Black J.H., Dalgarno A., 1976, ApJ 203, 132
Brand P.W., 1993, J. Chem. Soc. Faraday Trans. 89, 2131
Burton M.G., Bulmer M., Moorhouse A., Geballe T.R., Brand P.W.J.L., 1992, MNRAS 257, 1
Dalgarno A., 1993, J. Chem. Soc. Faraday Trans. 89, 2111
Draine B.T., Lee H.M., 1984, ApJ 285, 89
Duley W.W., Williams D.A., 1986, MNRAS 223, 177
Duley W.W., Williams D.A., 1993, MNRAS 260, 37
Eilmsteiner G., Walkner W., Winkler A., 1996, Surf. Sci. 352-354, 263; Eilmsteiner G., Winkler A., 1996, Surf. Sci. 366, L750
Field D., Gerin M., Leach S., et al., 1994, A&A 286, 909
Fitzpatrick E.L., Massa D., 1990, ApJS 72, 163
Fromherz T., Mendoza C., Ruette F., 1993, MNRAS 263, 851
Goodman F.O., 1978, ApJ 226, 87
Gough S., Schermann C., Pichou F., et al., 1996, A&A 305, 687
Hollenbach D.H., Salpeter E.E., 1970, J. Chem. Phys. 53, 79
Hollenbach D.H., Salpeter E.E., 1971, ApJ 163, 155
Hunter D.A., Watson W.D., 1978, ApJ 226, 477
Jackson B., Persson M., 1992a, J. Chem. Phys. 96, 2378
Jackson B., Persson M., 1992b, Surf. Sci. 269/270, 195
Jackson B., Persson M., 1995, J. Chem. Phys. 103, 6257
Jura M., 1975, ApJ 197, 575
Jura M., 1976, ApJ 204, 12
Klose S., 1989, Astron. nachr. 310, 409
Kratzer P., 1997, J. Chem. Phys. 106, 6752
Le Bourlot J., Pineau des forêts G., Roueff E., Dalgarno A., Gredel R., 1995, ApJ 449, 178
Lemaire J.L., Field D., Gerin M., et al., 1996, A&A 308, 895
Mathis J.S., Rumpl W., Nordsieck K.H., 1977, ApJ 217, 425
Mattera L., Rosatelli F., Salvo C., et al., 1980, Surf. Sci. 93, 515
Persson M., Jackson B., 1995a, Chem. Phys. Lett. 237, 468
Persson M., Jackson B., 1995b, J. Chem. Phys. 102, 1078
Pirronello V., Liu C., Shen L., Vidali G., 1997, ApJ 475, L69
Pirronello V., Biham O., Liu C., Shen L., Vidali G., 1997, ApJ 483, L131
Rettner C.T., 1994, J. Chem. Phys. 101, 1529
Rettner C.T., Auerbach D.J., 1994, Science 263, 365
Rettner C.T., Auerbach D.J., 1996, J. Chem. Phys. 104, 2732
Rouan D., Field D., Lemaire J.L., et al., 1997, MNRAS 284, 395
Ross S., Oliver J.P., *On Physical Adsorption* New-York: Interscience, 1964
Schermann C., Pichou F., Landau M., Čadež I., Hall R.I., 1994, J. Chem. Phys. 101, 8152
Schmoranzer H., Noll T., Roueff E., Abgrall H., Bieniek R., 1990, Phys. Rev. A 42, 1835
Stephens T.L., Dalgarno A., 1972, J. Quant. Spectrosc. Radiat. Transfer 12, 569
Sugai H., Malkan M.A., Ward M.J., Davies R.I., McLean I.S., 1997, ApJ 481, 186
Watson W.D., 1976, Rev. Mod. Phys. 48, 513
Wetzig D., Dopheide R., Rutkowski M., David R., Zacharias H., 1996, Phys. Rev. Lett. 76, 463